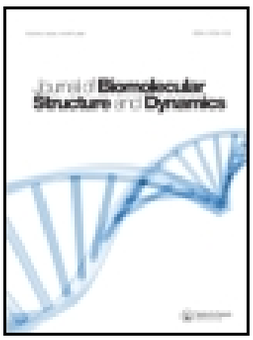

Taylor & Francis
Taylor & Francis Group

Journal of Biomolecular Structure and Dynamics

ISSN: 0739-1102 (Print) 1538-0254 (Online) Journal homepage: http://www.tandfonline.com/loi/tbsd20

Evaluation of (η^6-*p-cymene*)Ruthenium diclofenac complex as Anticancer Chemotherapeutic Agent: Interaction with Biomolecules, Cytotoxicity Assays

Rais Ahmad Khan, Hamad A. Al-Lohedan, Mohammad Abul Farah, Mohd. Sajid Ali, Ali Alsalme, Khalid Mashay Al-Anazi & Sartaj Tabassum

To cite this article: Rais Ahmad Khan, Hamad A. Al-Lohedan, Mohammad Abul Farah, Mohd. Sajid Ali, Ali Alsalme, Khalid Mashay Al-Anazi & Sartaj Tabassum (2018): Evaluation of (η^6-*p-cymene*)Ruthenium diclofenac complex as Anticancer Chemotherapeutic Agent: Interaction with Biomolecules, Cytotoxicity Assays, Journal of Biomolecular Structure and Dynamics, DOI: 10.1080/07391102.2018.1528180

To link to this article: https://doi.org/10.1080/07391102.2018.1528180

Accepted author version posted online: 26 Sep 2018.

Evaluation of (η^6-*p-cymene*)Ruthenium diclofenac complex as Anticancer Chemotherapeutic Agent: Interaction with Biomolecules, Cytotoxicity Assays.

Rais Ahmad Khan,[α] Hamad A. Al-Lohedan,[φ] Mohammad Abul Farah,[§] Mohd. Sajid Ali,[φ] Ali Alsalme,[α] Khalid Mashay Al-Anazi,[§] Sartaj Tabassum,[φ,*]

[φ]*Surfactant Research Chair,* [α]*Department of Chemistry, College of Sciences, King Saud University, P.O. Box 2455, Riyadh 11451, KSA.*

[§]*Department of Zoology, College of Sciences, King Saud University, Riyadh 11451, KSA.*

**Corresponding Author:* tsartaj62@yahoo.com, Mobile No. +966 530128012

Abstract

The designing of metal-based anticancer therapeutics agents can be optimized in a better and rapid way if the ligands utilized have standalone properties. Therefore, even when the organometallic/coordination complex (i.e., metallodrug) gets dissociated in extreme conditions, the ligand can endorse its biological properties. Herein, we have synthesized and characterized η^6-*p*-cymene ruthenium diclofenac complex. Furthermore, the ruthenium complex interactions with HSA and ct-DNA have been studied using various spectroscopic studies viz., UV, fluorescence, and circular dichroism and exhibited significant binding propensity. Furthermore, *in-vitro* cytotoxicity assays were carried out against human breast cancer "MCF-7" cell line. The η^6-*p*-cymene ruthenium diclofenac complex registered significant cytotoxicity with an IC_{50} value of ~25.0 μM which is comparable to the standard drugs. The η^6-*p*-cymene ruthenium diclofenac complex was able to decrease the MCF-7 cell proliferation and induced significant levels of apoptosis with relatively low toxicity.

Keywords: Ruthenium diclofenac complex; Biomolecular interaction; cytotoxicity against MCF7; Apoptosis.

1. Introduction

Metallo-chemotherapeutics is a well-established conventional selection for a wide range of diseases since ancient times, particularly for antibacterial, antifungal, analgesic, antipyretic and anti-cancer. After the serendipitous discovery of cisplatin and its derivatives, (Rosenberg, B., et.al.1967, 1969, 1977, 1978) the field of metal-based chemotherapeutics got triggered, and since then the field is evolved stalwartly. However, the acquired, intrinsic resistance and adverse side-effects have marred the remarkable success of platinum-based drug candidates (Gasser & Metzler-Nolte, et al., 2012; Barry, & Sadler, 2013; Galanski et al., 2003; Hill & Speer, 1982; Khan et al., 2014; Kelland et al., 2007).

In lieu of the problem of undesirable side effects and to improve efficacy, ruthenium complexes emerged as the potential class of anticancer agents. Among the Ru(III) compounds, NAMI-A (a metastasis agent), (imidazolium *trans*-[tetrachlorido(dimethyl sulfoxide)(1H-imidazole)ruthenate (III)] and KP1019, (indazolium *trans*-[tetrachloridobis(1H-indazole)ruthenate(III)] and KP1339, (sodium (indazolium *trans*-[tetrachloridobis(1H-indazole)ruthenate(III)] exhibited potential activity against human tumor models, are subjected to phase II clinical trials.(Hartinger, et al., 2012; 2008; 2006.) In recent decades, fluxional ruthenium arene complexes have emerged as versatile scaffolds for the design of the new metallodrugs (Mehta, et.al. 2017, Yadav, et al, 2018, Yaun, et. al., 2013). In this area of half sandwich-organoruthenium, groups of scientist viz, Sadler et al. (Zhang, & Sadler et.al. 2017; Bruijnincx, & Sadler et. al., 2009), Dyson

et al., (Nazarov, et. al., 2014; Murray, et.al, 2016) and Keppler et al., (Hartinger, et.al, 2006; Renfrew, et al., 2009) with their co-workers have marked a tremendous success with piano-stool type geometry. RAPTA-C [(η^6-*p*-cymene)Ru(PTA)Cl_2], PTA; 1,3,5-triaza-7-phosphatricyclo[3.3.1.1]decane and RM175 [Ru(η^6-biphenyl)(ethylene-diammine)Cl]$^+$ are the representatives of this class and hit the clinical trials with good impact. Merely having slight modifications in the structures of the two they exhibited extremely different biological properties. These lead molecular frameworks has been extensively modified at both the ends viz., arenes part as well as the co-ligand/s to build up a structural-activity relationship (SAR) and decorated with different functionalities to get target specificity of the drug candidates.

Interestingly, combination therapy has also emerged in scientist are working on the already existing drugs mainly NSAIDs, and combining with the metal centers and studying the synergistic effect of metallodrugs, which have shown significant potential. In organo-ruthenium complexes, Turel et al.(Hudej et al., 2012; Turel et al.,2010; Kljun et al., 2011) synthesized Ru(arene) complexes of antibacterial compounds viz, nalidixic acid, ofloxacin. Likewise, Aman et al. 2014, has developed ruthenium arene compounds with oxicam moieties namely, piroxicam and meloxicam (see fig 1).

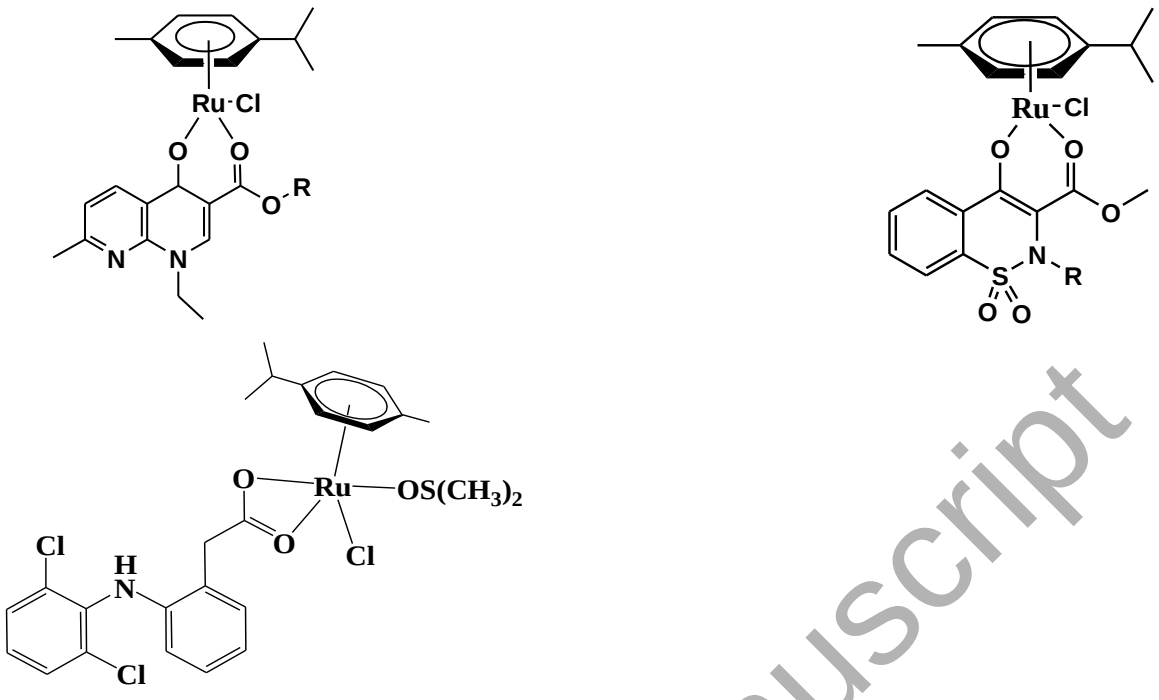

Turel et al. **Aman et al.** **Present work**

Figure 1. Structures of the representatives of this class of η^6-*p*-cymene ruthenium complexes

Thus standing on this, we have studied the η^6-*p*-cymene ruthenium derived diclofenac complex (**1**) as a potential metallo-chemotherapeutic agent. The binding affinity of ruthenium complex with DNA and HSA has also been studied using various spectroscopic techniques and calculating various binding parameters. Furthermore, this ruthenium complex was studied against MCF-7 human breast cancer cell lines via cytotoxicity assays, studying the apoptotic potential and morphological changes induced by the potential metallo-drug.

2. Experimental Section

2.1. Material and methods

The sodium salt of ct-DNA (D1501, Type I, fibers) and HSA essentially fatty acid-free (≥98%) were purchased from Sigma, USA. Tris(hydroxymethyl)aminomethane

hydrochloride (Tris-HCl) was of analytical grade and also obtained from Sigma. Fetal bovine serum (FBS), trypsin/EDTA and penicillin-streptomycin were purchased from Invitrogen (Carlsbad, CA, USA). Trypan blue, phosphate buffered saline (PBS), dimethyl sulfoxide (DMSO), ethidium bromide, acridine orange**,** and Dulbecco's Modified Eagle's medium (DMEM), were obtained from Sigma-Aldrich (St Louis, MO, USA). Cell Titer 96® Non-radioactive cell proliferation assay kit was obtained from Promega (Madison, WI, USA). Annexin V-FITC apoptosis detection kit was purchased from BD Biosciences (San Diego, USA). Culture wares and other consumables used in this study were procured from Nunc, Denmark

2.2. Biological Studies

2.2.1. HSA Binding Studies

HSA binding studies were carried out using UV-visible, fluorescence quenching and circular dichroism methods and the detailed experimental procedures for these studies have been described elsewhere (Alsalme, et al., 2016; Tabassum et al. 2017; Mach et al., 1995; Yusuf, et. al., 2018; Afzal, et al., 2018).

2.2.2. DNA Binding Studies

UV-visible spectroscopy, in the range of 225 to 350 nm, was used to understand the binding of η^6-*p*-cymene ruthenium diclofenac complex (**1**) with DNA. Increasing concentration of ct-DNA was titrated against 30 $x10^{-6}$ mol dm^{-3} of η^6-*p*-cymene ruthenium diclofenac complex. A fixed amount of ct-DNA (0-30 $x10^{-6}$ mol dm^{-3}) was taken in the blank and baseline was corrected before each measurement. The binding mode of the η^6-*p*-cymene ruthenium diclofenac complex was seen by competitive binding assay using EtBr and DAPI dyes. The circular dichroism studies of ct-DNA in the

presence of complex were carried out similarly as described in case of HSA binding. (Mach, et al., 1995; Tabassum et al., 2012; Khan et al., 2014; Yusuf, et. al., 2018; Afzal, et al., 2018)

2.2.3. Cell cultures, and in-vitro Cytotoxicity, Apoptosis Experiments

The MCF-7 human breast cancer cell culture, cytotoxicity and apoptosis experiments were carried out by using standard protocols as adopted by us (Farah et al., 2016) with slight modifications, for more detail see SI.

3. Result and discussion

3.1. Synthesis and Characterization

To synthesize the ruthenium η^6-arene NSAID compound (**1**), the sodium salt of diclofenac reacted with (η^6-*p-cymene*) ruthenium dichloride dimer was stirred in dry methanol and few drops of dimethyl sulfoxide. The mixture was stirred at 80 °C for 10 h, and the reaction mixture kept on slow evaporation. The yellow color precipitation in yield of 68% was obtained. Unfortunately, after several attempts, we are unable to grow suitable single crystals for X-ray study. However, the ruthenium compounds synthesized were characterized by several spectroscopic and analytical methods. Stability in aqueous medium and dmso is an essential requirement for drug candidates. Since dmso/water was used to make a stock solution for biological studies. The ruthenium compound was found quite stable in DMSO while in H_2O; the chlorine atom gets hydrolyzed and forms an aqua complex of ruthenium over a period of 1h (Fig 2).

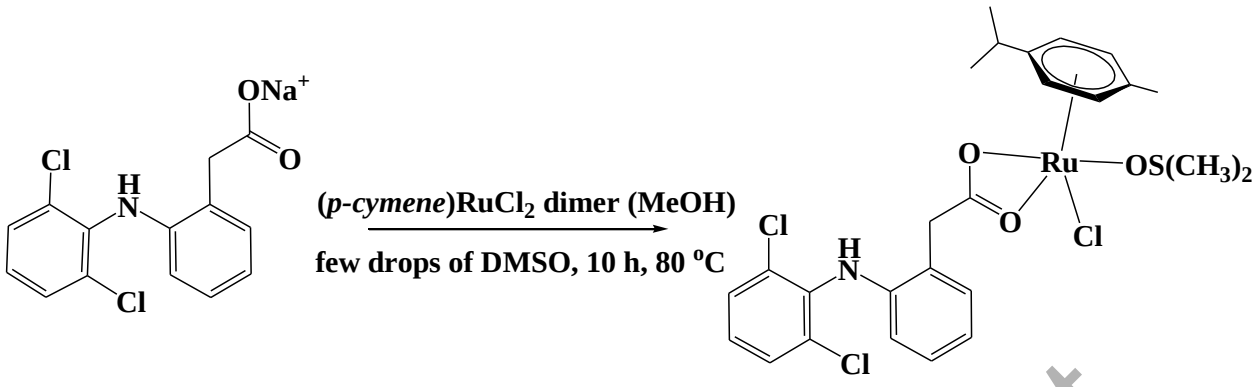

Figure 2. Schematic representation of the (η^6-p-cymene)ruthenium complex of diclofenac **(1).**

The FT-IR spectrum of the complex **1** showed ν_{asym} (C-O) and ν_{sym} (C-O) at 1567 and 1459 cm^{-1}, respectively which is characteristic for the bidentate coordination of carboxylate group of the ligand with a metal center. Since the difference between [ν_{asym} (CO) -ν_{sym} (CO)] is 108 cm^{-1}, which is less than 150 cm^{-1} and thus confirms the bidentate binding mode of the carboxylate moiety. The FT-IR spectrum exhibited absorption band at 1157, 976, 908 cm^{-1} exhibiting a significant shift in ν(S-O) corresponding to free DMSO (1005 cm^{-1}). Thus ascertains coordination of DMSO through sulfur to the metal center. The band at 438 cm^{-1} is attributed to the ν(Ru-O) (see Fig. S1, in ESI).

The ^{1}H NMR of the complex **1** in DMSO-d_6 resulted in significant shifts when compared to the ligand. Complexation with ligand is confirmed by the disappearance of the carboxylic O-H signal from 10.27 ppm and appearance of the *p*-cymene protons additional signals. An upfield shift of the signals of 0.7-0.5 ppm of the ligand was observed in the ligand upon complexation. The band associated with the DMSO coordinated with the metal center and in solution due to the dissociation of the labile

chlorido is also quite evident and which leads to the formation of a most stable product which is ascertained by the ESI-MS of the complex (see Fig. S2-S6 in SI).

The UV-Vis spectrum of the ligand exhibited the band at around ~275 nm (n-π* transition) and upon complexation, the complex **1** displayed the band complex at ~260 nm with a significant shift of around 15 cm^{-1} and the new band appears at 323 nm (LMCT band) which confirms the coordination. The emission spectrum of the ruthenium complex was also taken in solution and found exhibit signals at ~360 nm (see Fig S8, S9 in SI).

3.2. Biological Studies

3.2.1. HSA Binding Studies

The difference UV-visible spectra of HSA with various concentrations of the complex **1** are shown in Fig 3.

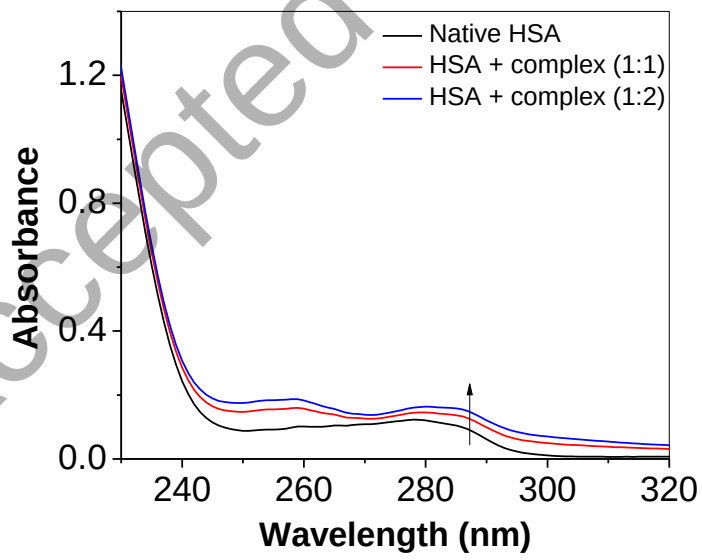

Figure 3. Difference UV – visible spectra of HSA-complex binding. [HSA]=3 μM

HSA gives a peak at 280 nm which can be used to see the changes during its binding with the ligand (Mach et al., 1995). The increased intensity of the protein-Ru-Diclofenac system in comparison to the pure HSA is an indication of the complex formation between HSA and Ru-diclofenac; moreover, a noticeable red shift of the absorption maximum is due to the involvement of electrostatic interaction.

The fluorescence intensity of HSA decreases gradually (Ali et al. 2017) with the increase in the concentration of Ru-Diclofenac complex (Fig. 4). Since there is a significant redshift of about 11 nm in the maximum fluorescence emission at a wavelength, it is proposed that the involvement of electrostatic interactions (Mandeville et al., 2009).

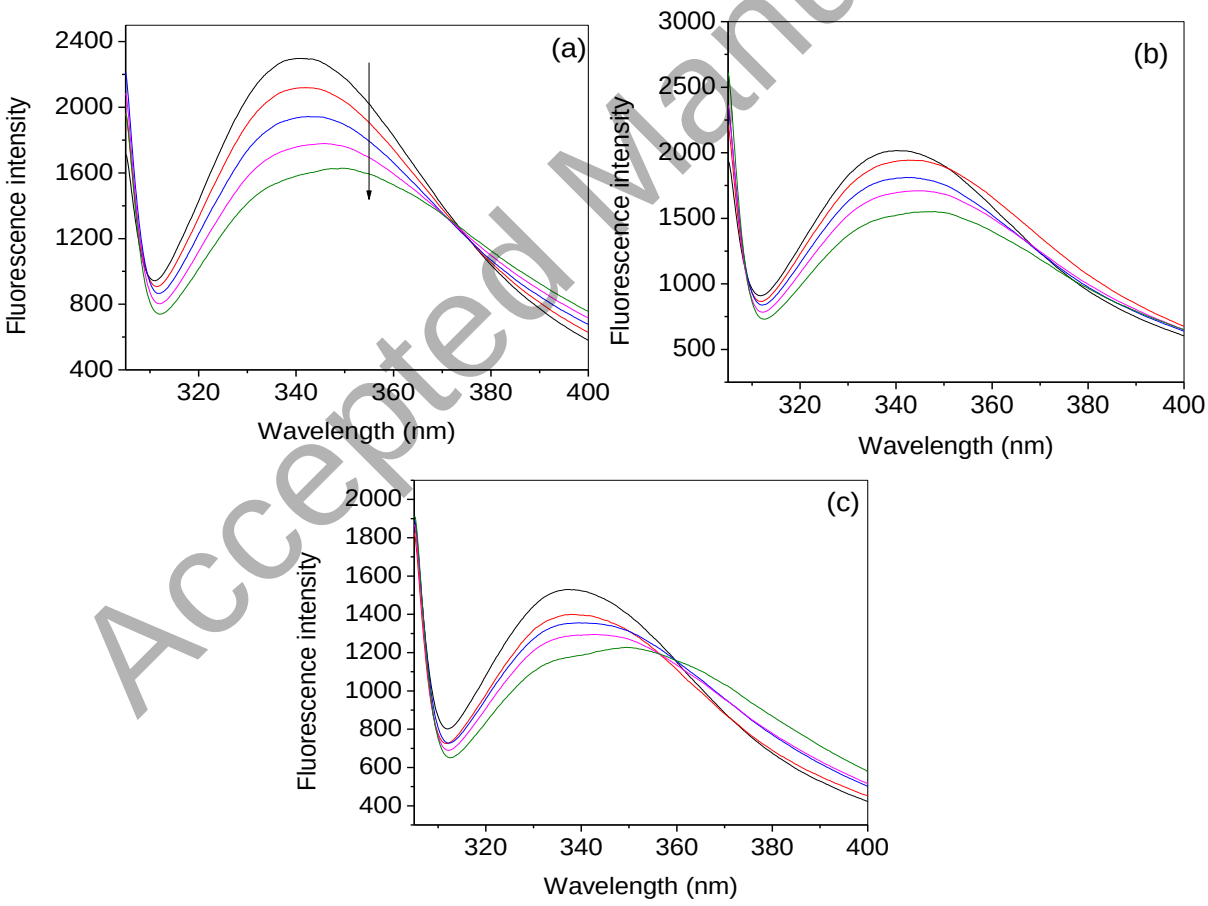

Figure 4. Effect of complex **1** on the fluorescence emission spectra (λ_{ex} = 295 nm) of HSA at (a) 25 °C, (b) 35 °C and (c) 45 °C. [HSA] = 3 µM, [complex] = 0, 2.5, 5, 7.5, 10, µM.

Various fluorescence and binding parameters have been calculated using Figs. 5 & 6 and Eqs. (S1-S3) (For equations, see SI) and their values are summarized in Table 1 (Lakowicz, et al., 1999; Anand et al., 2010).

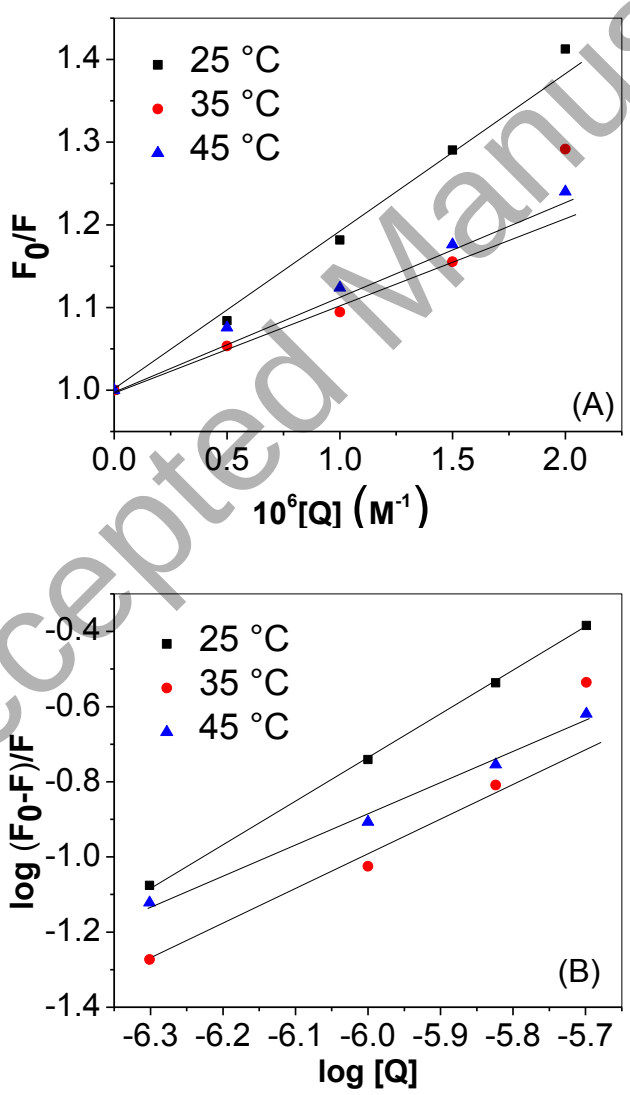

Figure 5.(A) Stern-Volmer plots of HSA interaction with complex **1** at various temperatures. [HSA] = 3 μM, λex=295 nm. (B) Plot of log $(F_0 - F)/F$ as a function of log [complex]. [HSA] = 3 μM, λex=295 nm.

Decreasing trend of the Stern-Volmer constant demonstrates the involvement of the static type of quenching mechanism. Binding parameters were computed using Eq 3 and Fig. 5 (B) the data are displayed in Table 1. There was approximately 1:1 binding between HSA and complex **1**. The thermodynamic parameters (change in enthalpy (Δ*H*), entropy (Δ*S*) and free energy change (Δ*G*)) were calculated adopting the widely used Van't Hoff equation Usman et al. 2017, for which the plot is given in Fig. 6.

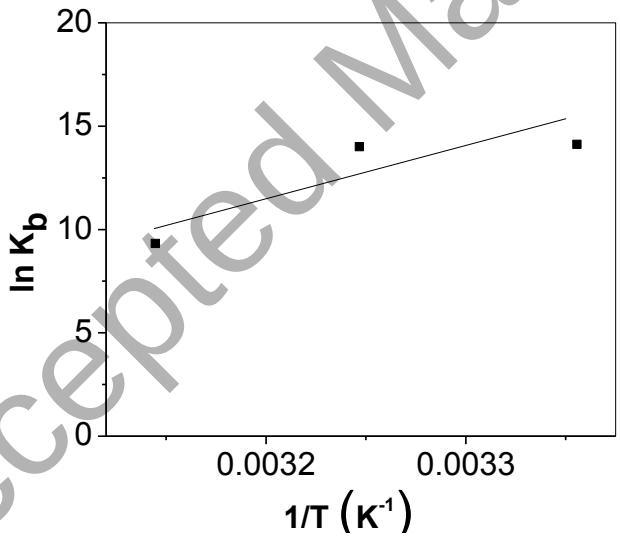

Figure 6. Van't Hoff plot of HSA interaction with the complex **1**. [HSA] = 3 μM, λ_{ex}=295 nm.

The values of thermodynamic parameters, calculated by Eqs. S4 and S5 (for equations, see SI) using Fig. 6 are given in Table 1, and it is clear from the negative values of ΔG

that the binding of complex **1** with HSA is a spontaneous process. The interaction is also a highly exothermic process with a substantial ordering of the system as revealed by the negative values of both ΔH and ΔS.

Table 1 Stern-Volmer quenching constants, binding parameters and thermodynamic parameters for the interaction of HSA with complex **1** at various temperatures. λ_{ex}= 295nm

T (K)	Stern-Volmer quenching constants			Binding parameters			Thermodynamic Parameters		
	K_{sv} (M^{-1})	K_q ($M^{-1}s^{-1}$)	R^2	n	K (M^{-1})	R^2	ΔG (KJ mol^{-1})	ΔH (KJ mol^{-1})	ΔS (J mol^{-1} K^{-1})
288	1.97 x 10^5	3.45 x 10^{13}	0.9924	1.1	13.6 x 10^5	0.9996	-36.87	-187.27	-504.69
298	1.25 x 10^5	2.19 x 10^{13}	0.9247	1.1	12.0 x 10^5	0.9529	-31.82		
308	1.20 x 10^5	2.10 x 10^{13}	0.9921	0.9	1.1 x 10^5	0.9921	-26.78		

The far-UV CD is a useful method to determine the secondary structure of proteins (Ali et al. 2016). The far-UV CD spectra of HSA in absence and presence of complex **1** are given in Fig.7.

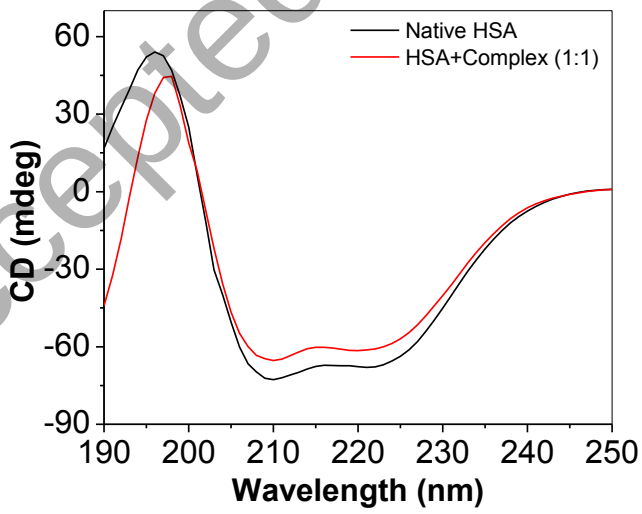

Figure 7. Far-UV CD spectra of HSA in the presence of complex **1** at 25 °C and pH 7.4. [HSA] = 3 µM.

It is exhibited from the figure that ellipticity of HSA is decreasing in the presence of the complex. Hence, it can be deduced that HSA partially unfolds in the presence of complex **1** (Feng et al., 1998).

3.2.2. DNA Binding Studies

UV-visible spectroscopy is an important technique to obtain the information about ligand-biomolecules interactions. Difference UV-visible spectra of ct-DNA and complex **1** interaction are given in Fig.8 addition of ct-DNA to the **1** cause's slight hypochromism in the spectra.

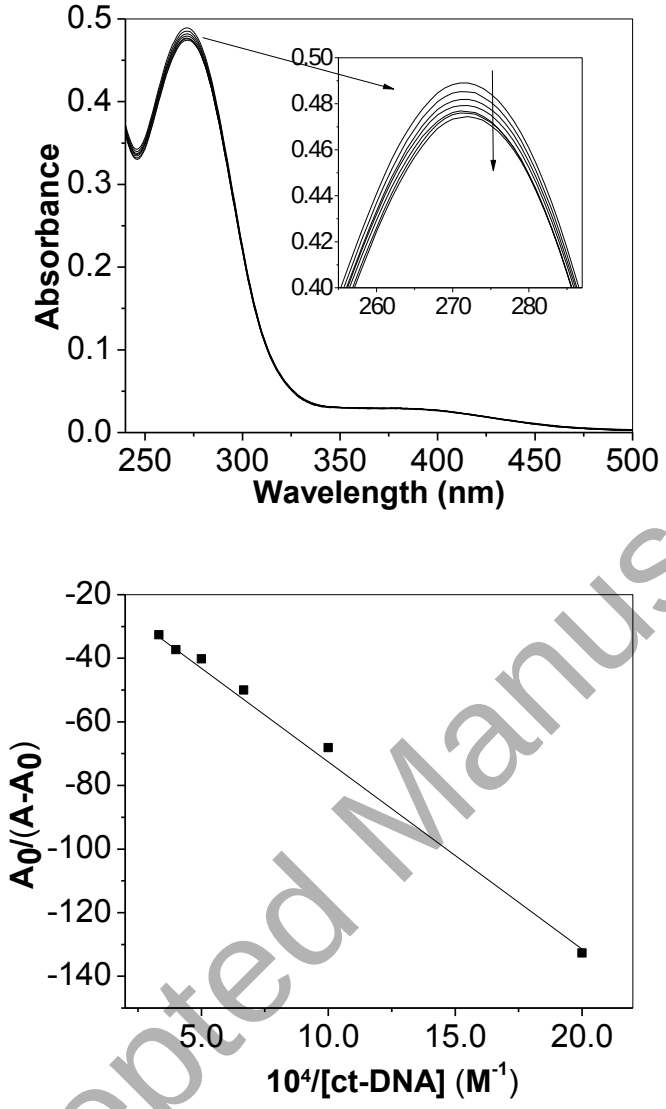

Figure 8. (a) UV–visible absorption spectra of ct-DNA (30 µM) in the presence of increasing concentrations of the complex **1** (0-30.0 µM) at 25 °C. (b) Figure showing Benesi Hildebrand plot.

The changes in the absorbance at 278 nm were utilized to calculate the apparent association constant, K_{app}, of **1** and ct-DNA interaction.

$$\frac{1}{A_{obs} - A_0} = \frac{1}{A_c - A_0} + \frac{1}{K_{app}(A_c - A_0)[ct - DNA]} \qquad (4)$$

A graph of $1/(A_{obs} - A_0)$ versus 1/[ct-DNA] yielded a Benesi Hildebrand (B-H) plot with a slope equal to $1/K_{app}$ $(A_C - A_0)$ and an intercept equal to $1/(A_C - A_0)$. From the plot, the values of K_{app} was found to be 1.85 x 10^4 M^{-1}.

From the collective information obtained from the DAPI and EtBr displacement assays, Fig 9. It is proposed that the complex **1** bound at the interfacial region of minor groove and intercalation site.

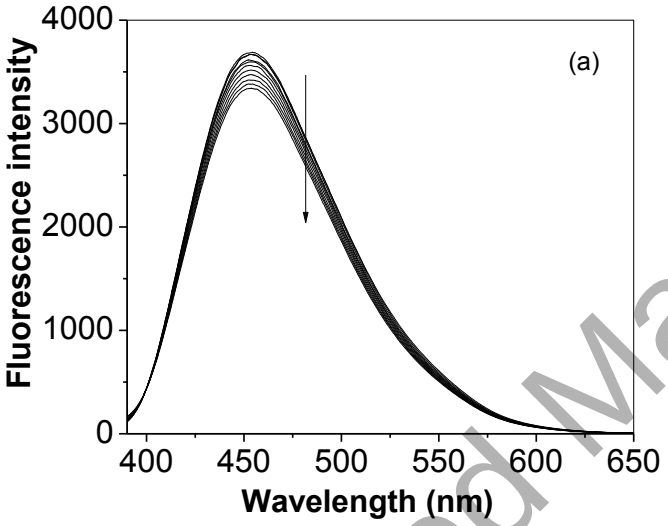

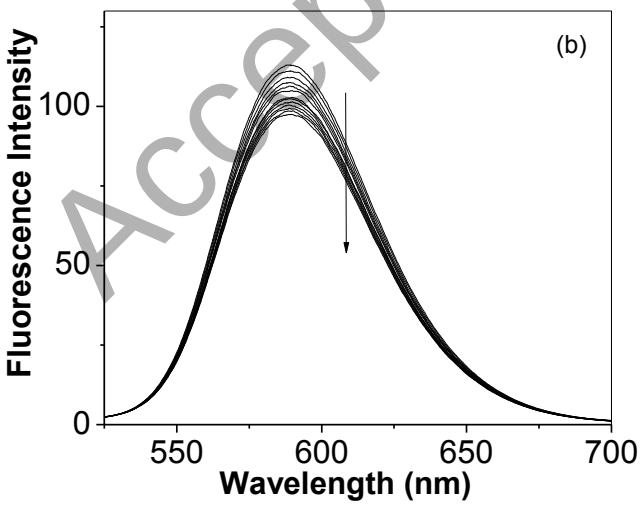

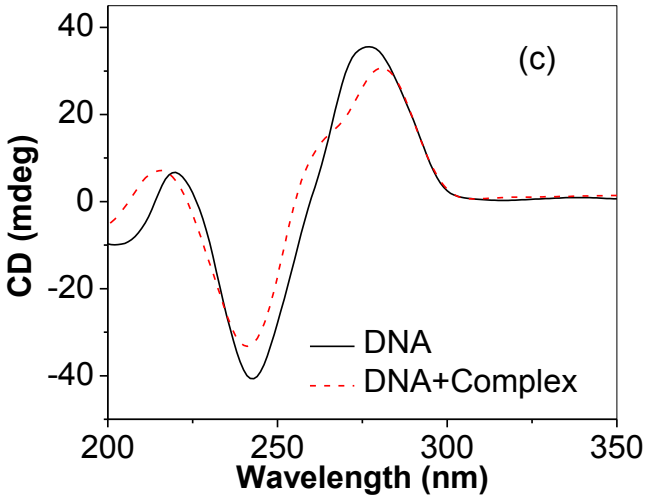

Figure 9.**(**a) Fluorescence titration of CT-DNA and DAPI complex with the complex **1**. (b) Fluorescence titration of EtBr and ct-DNA with complex **1**. (c) CD spectra of DNA in absence and presence of the complex **1**. The concentration of [DNA] =30 µM and [complex] =10 µM.

3.2.3. Cytotoxicity Assay

The percent viability of cells exposed to different concentrations of complex **1** and ruthenium dimer (**R**) (5.0-50.0 µM). The IC_{50} values estimated at 24 h post-treatment in MCF-7 for complex **1** is about 25.0 µM and for **R** is ~400 µM. A significant ($p < 0.05$) decrease in the cell viability was observed which was also concentration dependent. At the highest concentration of 50.0 µM cell proliferation was inhibited by 77% and 59% with complex **1** and **R** (ruthenium salt) treatment, respectively. While at lowest concentration of 5.0 µM 79% and 88% percent cell growth was registered for complex **1** and **R** treatment, respectively. These data suggest that complex **1** induced higher cytotoxicity in MCF-7 cells as compared to standard drugs (cisplatin IC_{50}= 28±0.6 µM, Morais et el, 2012). Ruthenium complexes reported earlier exhibited IC_{50} values against

MCF7 cell line, $[Ru(bpy)_2\ p\text{-}CPIP]^{2+}$, IC_{50} = 64.4 µM; $[Ru(bpy)_2\ p\text{-}NPIP]^{2+}$, IC_{50} = 86.5 µM; $[Ru(phen)_2\ p\text{-}NPIP]^{2+}$, IC_{50} = 38.9 µM (Perdisatta et al 2018) in comparision to these complex **1** exhibited significantly good activity.

3.2.4. Morphological changes analysis

To evaluate any morphological changes in MCF-7 cells induced by complex **1**, cells were treated with two concentrations below IC_{50} value for complex **1** (5.0 and 10.0 µM) for 24h. Fig. 10 shows inverted microscopic images of morphological alterations observed in MCF-7 cells. The untreated control cells (Fig. 10 A) reached about 95-100% confluence contained a typical shape and was found attached to the surface. Conversely, in the treated groups the cells lost their normal epithelial cell morphology, becoming elongated, and some of them found swelled condition. A significant decrease in cell population was observed in complex **1** treated MCF-7 cells (Fig. 10 B-C).

Figure 10. Phase contrast inverted microscopic observation of MCF-7 cells for morphological alterations induced by complex **1** (B, C). (A) Control (B) 5.0 µM (C) 10.0 µM. Magnification: 100X

3.2.5. Detection of Apoptosis by flow cytometry

The percentages of early and late apoptotic and necrotic cells were measured using flow cytometry to quantify the levels of detectable phosphatidylserine on the outer membrane

of apoptotic cells (Evens et al., 2004). Representative results in the form of dot plots were presented in fig. 11.

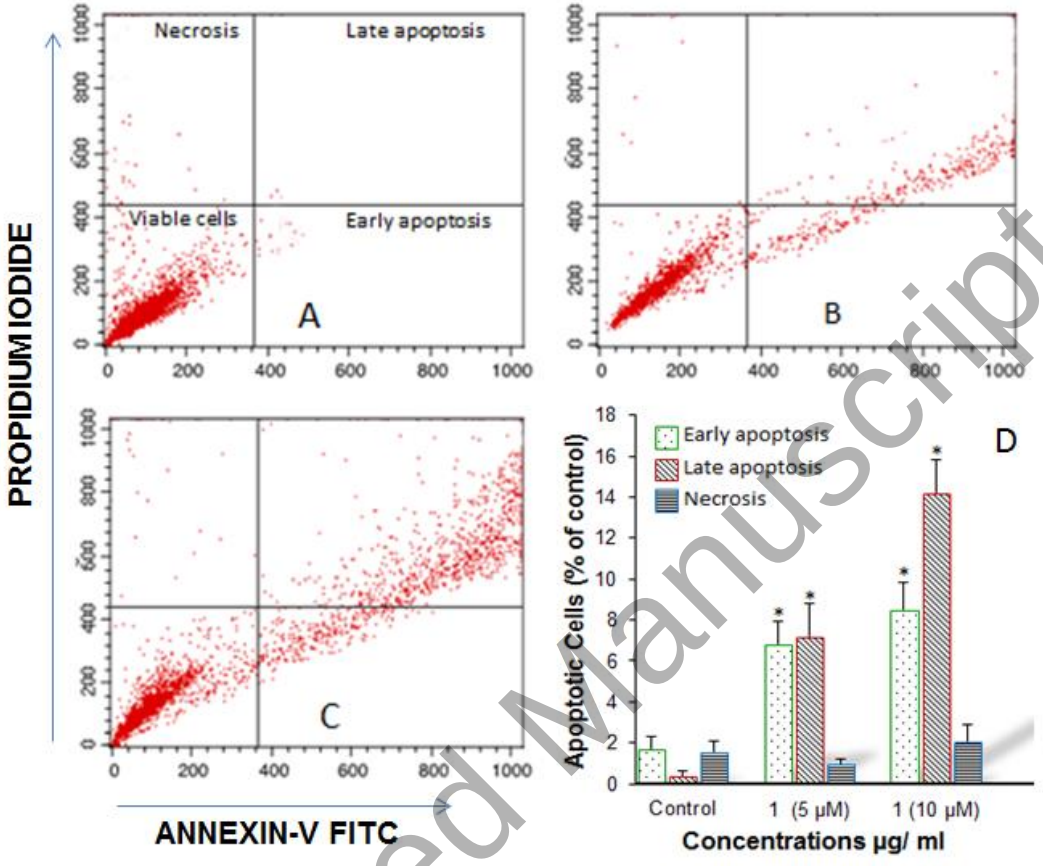

Figure 11. Flow cytometric analysis of MCF-7 cells exposed to different concentrations of complex **1** (B, C) for 24 h. Representative dot plots showing the percentage of viable cells, early apoptosis, late apoptosis and necrotic cells (A) Control, (B) 5.0 µM (C) 10.0 µM (D) Bar diagrams showing the percentage of apoptosis observed by flow cytometric analysis of MCF-7 cells. All data are expressed as mean ± SE. * Significant ($p < 0.05$) compared with controls.

The treatment of MCF-7 with complex **1** revealed that a significant decrease ($p < 0.05$) in the population of viable cells and increase in the percentage of apoptotic cells was observed. While in the untreated control, the only small percentage of apoptotic cells was

observed (Fig. 11 A). As seen in figure 11, MCF-7 cells when exposed to **1**, the percentage of early apoptosis cells increased to 7.2% in 5.0 µM to 14.2% 10.0 µM concentrations. While, the percentage of late apoptosis cells reached 9.5% and 7.8% in 5.0 µM and 10.0 µM, respectively (Figure 11 B-C).

3.2.6. Apoptotic morphological changes in MCF-7 cells

MCF-7 cells were exposed to complex **1** for 24 h as mentioned above and stained with acridine orange/ ethidium bromide (AO/EB) dye to test if the increase in cell death was due to apoptosis (Fig. 12).

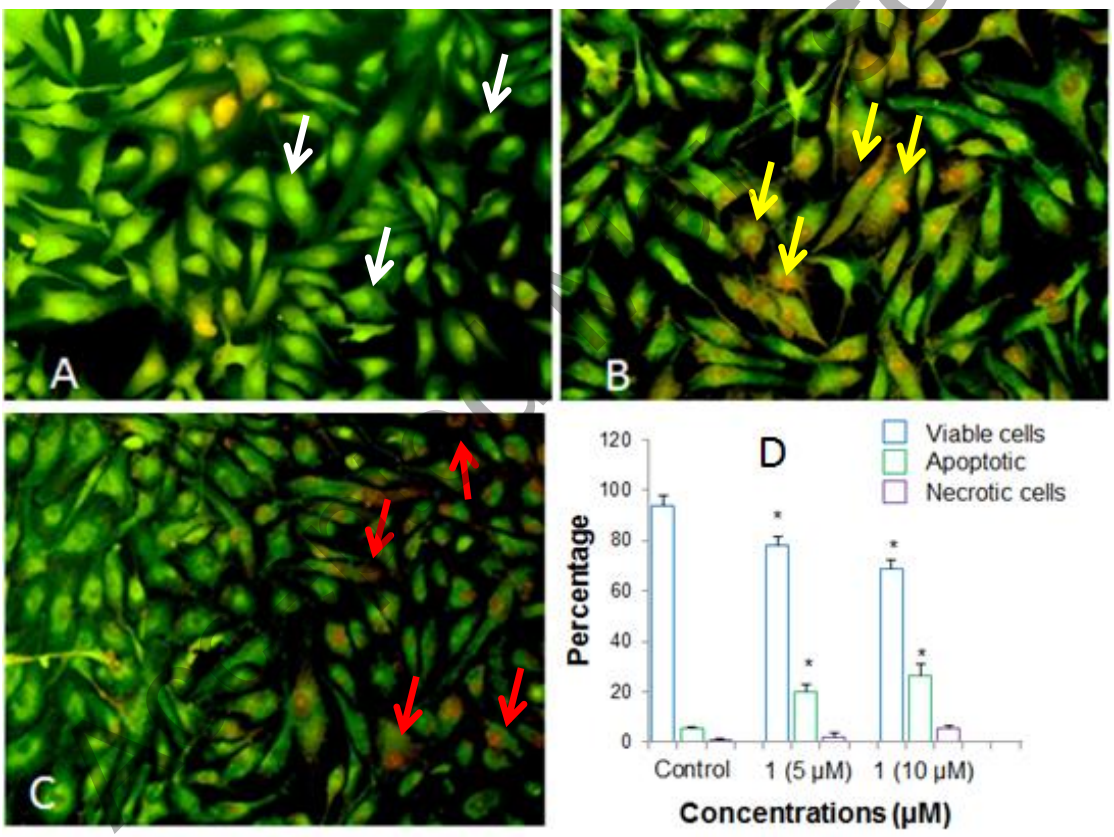

Figure 12. Apoptotic morphological changes in MCF-7 cells observed under fluorescence microscopy. (A) Control (B) 5.0 µM **1** (C) 10.0 µM **1**. Magnification: 200X. (F) Quantification of normal, apoptotic and necrotic cells recorded in more than 300 cells. All data are expressed as mean ± SE for three independent experiments. * Significant (*p*

< 0.05) compared with control. Note: White arrows: Viable cells (living cells); Yellow arrows: Apoptotic cells; Red arrows: Necrotic cells

AO/EB staining facilitates typical apoptotic nuclear morphology such as nuclear shrinkage, DNA condensation, and fragmentation. Around 93.7% of viable cells were prominently evident in untreated MCF-7 cells. Control cells showed uniformly distributed green fluorescence (AO stain) with no morphological changes and no red fluorescence (Fig 12A). The percentage of viable cells, however, decreased significantly ($p < 0.05$) in both the treatments. As shown in Fig 12 B-C, and D. Quantification of apoptotic and necrotic cells in total 300 cells in each group were performed which revealed that complex **1** treatment induced highest percentage of apoptotic cells (26.2%). The MTT assays, AO/EB staining, and flow cytometry analysis showed similar concentration and time-dependent effects on MCF-7 cells. There was a difference in the percentage of viable cells because MTT is based on mitochondrial function assays that detected cell death earlier than others, while apoptosis is indicating assays (AO/EB and flow cytometry) detected cell death later in the process, which is in correlation with other reports (Curčić et. al., 2012; Oh et. al., 2004). The AO/EB method improves the detection of apoptosis and can distinguish between late apoptotic and dead cells. (Liu et al., 2015)

4. Conclusion

A new methodology was adopted for the search of the potential new drug with known bioactive compounds. In our studies, we have designed and synthesized a new potential metallodrug with use of sodium diclofenac (an anti-inflammatory drug) as bioactive ligand and coordinated it with the metal core, i.e., ruthenium(*p*-cymene) with known

anticancer properties. The binding propensity of the ruthenium complex **1** with model protein (HSA) and ct-DNA was investigated. The ruthenium complex **1** binding results exhibited significant binding propensity via interfacial binding mode. Furthermore, the ruthenium complexes were studied for cytotoxicity against MCF-7 (breast cancer cell lines) and the IC_{50} values are compared with the standard drug cisplatin and earlier reported ruthenium complexes and ruthenium complex **1** exhibited significantly good activity. From these experimental data, we infer that the ruthenium complex **1** possess potential to act as anti-cancer agent. The results warrants further detail investigations and we anticipate that our findings of drug designing will contribute to the search of new anticancer drugs.

Acknowledgment

The authors are grateful to the Deanship of Scientific Research, King Saud University for funding through Vice Deanship of Scientific Research Chairs.

References

Afzal, M., Al-Lohedan, H. A., Usman, M., & Tabassum S., (2018). Carbohydrate-based heteronuclear complexes as topoisomerase Iα inhibitor: approach toward anticancer chemotherapeutics, *J. Biomol. Struct. Dyn.*., (Accepted) https://doi.org/10.1080/07391102.2018.1459321.

Ali, M.S., Al-Lohedan, H.A., (2013). Sulfadiazine binds and unfolds bovine serum albumin: an in vitro study. *Mol. Biol. Rep.*, *40*, 6081-6090. DOI: https://doi.org/10.1007/s11033-013-2719-8.

Ali, M. S., Al-Lohedan, H. A., (2017). Deciphering the interaction of procaine with bovine serum albumin and elucidation of binding site: A multi spectroscopic and molecular docking study. *J. Mol. Liq., 236,* 232–240. DOI: https://doi.org/10.1016/j.molliq.2017.04.020.

Ali, M. S., Al-Lohedan, H. A., (2016). Multi-technique approach on the interaction between sugar-based surfactant n-dodecyl β-D-maltoside and bovine serum albumin. *J. Lumines., 169,* 35–42. DOI: https://doi.org/10.1016/j.jlumin.2015.08.049.

Anand, U., Jash, C., Mukherjee, S., (2010). Spectroscopic Probing of the Microenvironment in a Protein−Surfactant Assembly. *J. Phys. Chem. B, 114.* 15839-15845. DOI: 10.1021/jp106703h.

Aman, F., Hanif, M., Siddiqui, W. A., Ashraf, A., Filak, L. K., Reynisson, J., Söhnel, T., Jamieson, S. M. F., & Hartinger, C. G. (2014). Anticancer Ruthenium(η6-p-cymene) Complexes of Nonsteroidal Anti-inflammatory Drug Derivatives. *Organometallics, 33,* 5546–5553. DOI: 10.1021/om500825h.

Alsalme, A., Laeeq, S., Dwivedi, S., Khan, M. S., AlFarhan, K., Musarrat, J., & Khan, R. A. (2016). Synthesis, characterization of α-Amino acid Schiff base derived Ru/Pt complexes: induces cytotoxicity in HepG2 cell via protein binding and ROS generation. *Spectrochim, Acta A, 163,* 1–7. DOI: https://doi.org/10.1016/j.saa.2016.03.012

Bruijnincx, P.C.A., & Sadler, P. J. (2009). Controlling platinum, ruthenium and osmium reactivity for anticancer drug design. *Adv. Inorg. Chem., 61,* 1-62. DOI: 10.1016/S0898-8838(09)00201-3.

Barry, N. P. E., & Sadler, P. J. (2013). Exploration of the medical periodic table: towards new targets. *Chem. Commun.* 49, 5106–5131. DOI: 10.1039/C3CC41143E.

Curčić, M.G., Stanković, M.S., Mrkalić, E.M., Matović, Z.D., Banković, D.D., Cvetković, D.M., Dačić, D.S., & Marković, S.D. (2012). Antiproliferative and proapoptotic activities of methanolic extracts from Ligustrum vulgare. L. as an individual treatment and in combination with palladium complex. *Int. J. Mol. Sci., 13,* 2521-2534. DOI: 10.3390/ijms13022521.

Evens, A.M., Prachand, S., Shi, B., Paniaqua, M., Gordon, L.I., & Gartenhaus, R.B. (2004). Imexon-Induced Apoptosis in Multiple Myeloma Tumor Cells is Caspase-8 Dependent. *Clin. Cancer Res., 10,* 1481-1491. DOI: 10.1158/1078-0432.CCR-1058-03.

Farah, M. A., Ali, M.A., Chen, S. M., Li, Y., Al-Hemaid, F.M., Abou-Tarboush, F. M., Al-Anazi, K.M., Lee, (2016). Silver nanoparticles synthesized from Adenium obesum leaf extract induced DNA damage, apoptosis and autophagy via generation of reactive oxygen species *J. Colloids Surf. B Biointerfaces, 141,* 158-169. DOI: 10.1016/j.colsurfb.2016.01.027.

Feng, X.Z., Lin, Z., Yang, L.J., Wang, C., & Bai, C.L. (1998). Investigation of the interaction between acridine orange and bovine serum albumin. *Talanta 47* 1223-1229. https://doi.org/10.1016/S0039-9140(98)00198-2.

Gasser, G., & Metzler-Nolte, N. (2012). The potential of organometallic complexes in medicinal chemistry. *Curr. Opin. Chem. Biol., 16,* 84–91. DOI: 10.1016/j.cbpa.2012.01.013.

Galanski, M., Arion, V. B., Jakupec, M. A., & Keppler, B. K., (2003). Recent developments in the field of tumor-inhibiting metal complexes. *Curr. Pharm. Des., 9*, 2078–2089. DOI : 10.2174/1381612033454180.

Hartinger, C. G., Metzler-Nolte, N., & Dyson, P. J., (2012). Challenges and Opportunities in the Development of Organometallic Anticancer Drugs. *Organometallics, 31,* 5677−5685. DOI: 10.1021/om300373t.

Hartinger, C. G., Jakupec, M. A., Zorbas-Seifried, S., Groessl, M., Egger, A., Berger, W., Zorbas, H., Dyson, P. J., & Keppler, B. K. (2008). KP1019, a new redox-active anticancer agent--preclinical development and results of a clinical phase I study in tumor patients. *Chem. Biodiver., 5,* 2140−2155. DOI: 10.1002/cbdv.200890195.

Hartinger, C. G., Zorbas-Seifried, S., Jakupec, M. A., Kynast, B., Zorbas, H., & Keppler, B. K. (2006). From bench to bedside--preclinical and early clinical development of the anticancer agent indazolium trans-[tetrachlorobis(1H-indazole)ruthenate(III)] (KP1019 or FFC14A). *J. Inorg. Biochem., 100,* 891−904. DOI: 10.1016/j.jinorgbio.2006.02.013.

Hill, J. M., & Speer, R. J. (1982). Organo-platinum complexes as antitumor agents. *Anticancer Res., 2,* 173–186.

Hudej, R., Kljun, J., Kandioller, W., Repnik, U., Turk, B., Hartinger, C. G., Keppler, B. K., Miklavčič, D., & Turel, I. (2012). Synthesis and Biological Evaluation of the Thionated Antibacterial Agent Nalidixic Acid and Its Organoruthenium(II) Complex *Organometallics, 31,* 5867−5874. DOI: dx.doi.org/10.1021/om300424w

Khan, R. A., Arjmand, F., Tabassum, S., Monari, M., Marchetti, F., Pettinari, C. (2014). Organometallic ruthenium(II) scorpionate as topo IIα inhibitor; in vitro binding

studies with DNA, HPLC analysis and its anticancer activity. *J. Organomet. Chem., 771,* 47-58. DOI: 10.1016/j.jorganchem.2014.05.013

Khan, R. A., Yadav, S., Hussain, Z., Arjmand, F., & Tabassum, S., (2014). Carbohydrate linked Organotin (IV) Complexes as Human Topoisomerase Iα inhibitor and their antiproliferative effects against human carcinoma cell line (Huh7) by transcriptional regulation of specific gene. *Dalton Trans. 43,* 2534–2548. DOI: 10.1039/c3dt51973b.

Kelland, L. (2007). The resurgence of platinum-based cancer chemotherapy, *Nat. Rev. Cancer*, *7,* 573−584. DOI: 10.1038/nrc2167.

Kljun, J., Bytzek, A. K., Kandioller, W., Bartel, C., Jakupec, M. A., Hartinger, C. G., Keppler, B. K., & Turel, I. (2011). Physicochemical studies and anticancer potency of ruthenium η-p-cymene complexes containing antibacterial quinolones. *Organometallics*, *30,* 2506−2512. DOI: 10.1021/om101180c.

Lakowicz, J.R., (1999).Principles of Fluorescence Spectroscopy, Springer, New York 3rd edition.

Liu, K., Liu, P.C., Liu, R., & Wu, X., (2015). Dual AO/EB staining to detect apoptosis in osteosarcoma cells compared with flow cytometry. *Med. Sci. Monit. Basic Res., 21*, 15-20. DOI: 10.12659/MSMBR.893327

Mach, H., Volkin, D.B., Burke, C.J., & Middaugh, C.R. (1995). Ultraviolet absorption spectroscopy. In: Shirley BA (ed) Protein stability and folding: theory and practice, methods in molecular biology, Humana Press, Totowa, 40, 91–114.

Mandeville, J.-S., Froehlich, E., & Tajmir-Riahi, H.A., (2009). Study of curcumin and genistein interactions with human serum albumin. *J. Pharm. Biomed. Anal., 49,* 468-474. DOI: 10.1016/j.jpba.2008.11.035.

Mehta, J. V., Gajera, S. B. & Patel, M. N. (2017). Biological applications of pyrazoline-based half-sandwich ruthenium(III) coordination compounds, *J. Biomol. Struct. Dyn..*, *35*, 1599-1607. DOI: 10.1080/07391102.2016.1189360

Morais, T. S., Silva, T. J.L., Marques, F., Robalo, M. P., Avecilla, F., Madeira, P. J. A., Mendes, P. J.G., Santos, I., Garcia, M. H. (2012) Synthesis of organometallic ruthenium(II) complexes with strong activity against several human cancer cell lines. *J. Inorg. Biochem. 114*, 65–74. DOI: 10.1016/j.jinorgbio.2012.04.014

Murray, B. S., Babak, M. V., Hartinger, C. G., & Dyson, P. J. (2016). The development of RAPTA compounds for the treatment of tumors. *Coord. Chem. Rev., 306*, 86-114. DOI: 10.1016/j.ccr.2015.06.014

Nazarov, A.A., Hartinger, C.H., Dyson P. J., (2014). Opening the lid on piano-stool complexes: an account of ruthenium(II)–arene complexes with medicinal applications. *J. Organomet. Chem.*, *751*, 251-260. DOI: https://doi.org/10.1016/j.jorganchem.2013.09.016

Oh, H., Livingston, R., Smith, K., & Abrishamian-Garcia, L. (2004). *MIT Undergranduate Res. J.*, *11*, 53–62.

Perdisatt, L., Moqadasi, S., O'Neill, L., Hessman, G., Ghion, A., Qasim, M., Warraich, M., Casey, A., O'Connor, C., (2018).Synthesis, characterisation and DNA intercalation studies of regioisomers of ruthenium (II) polypyridyl complexes, *J. Inorg. Biochem. 182*, 71-82. DOI: https://doi.org/10.1016/j.jinorgbio.2018.01.018

Renfrew, A. K., Phillips, A. D., Egger, A. E., Hartinger, C. G., Bosquain, S. S., Nazarov, A. A., Keppler, B. K., Gonsalvi, L., Peruzzini, M., & Dyson, P. J. (2009). Influence of Structural Variation on the Anticancer Activity of RAPTA-Type

Complexes: ptn versus pta. *Organometallics*, *28*, 1165–1172. DOI: 10.1021/om800899e.

Rosenberg, B., VanCamp, L., Grimley, E. B., & Thomson, A. J. (1967). The inhibition of growth or cell division in Escherichia coli by different ionic species of platinum(IV) complexes. *J. Biol. Chem.*, *242*, 1347–1352.

Rosenberg, B., VanCamp, L., Trosko, J. E., & Mansour, V. H. (1969). Platinum Compounds: a New Class of Potent Antitumour Agents. *Nature*, *222*, 385–386.

Rosenberg, B. (1977). Noble metal complexes in cancer chemotherapy. *Adv. Exp. Med. Biol.*, *91*, 129–150

Rosenberg, B. (1978). Platinum complexes for the treatment of cancer. *Interdiscip. Sci. Rev.*, *3*, 134–147.

Tabassum, S., Afzal, M., Al–Lohedan, H., Zaki, M., Khan, R. A., & M. Ahmad, (2017). Synthesis and Structure Elucidation of New Open Cubane Tetranuclear [CuII4] Clusters: Evaluation of the DNA/HSA Interaction and pBR322 DNA Cleavage Pathway. *Inorg. Chim. Acta*, *463*, 142–155. DOI: https://doi.org/10.1016/j.ica.2017.04.031.

Tabassum, S., Parveen, M., Ali, A., Alam, M., Ahmad, A., Khan, A.U., & Khan, R.A. (2012). Synthesis of Novel Aryl-1,2,4,5-tetrazinane-3-thiones, *in-vitro* DNA Binding Studies, Nuclease Activity and its Antimicrobial activity. *J. Mol. Struct.*, *1020*, 33-40. DOI: https://doi.org/10.1016/j.molstruc.2012.03.049

Turel, I., Kljun, J., Perdih, F., Morozova, E., Bakulev, V., Kasyanenko, N., Byl, J. A. W., & Osheroff, N. (2010). First ruthenium organometallic complex of antibacterial agent

ofloxacin. Crystal structure and interactions with DNA. *Inorg. Chem. 49*, 10750−10752. DOI: 10.1021/ic101355d.

Usman, M., Zaki, M., Khan, R.A., Alsalme, A., Ahmad, M., Tabassum, S. (2017). Coumarin centered copper(II) complex with appended-imidazole as cancer chemotherapeutic agents against lung cancer: molecular insight via DFT-based vibrational analysis. *RSC Adv., 7*, 36056-36071. DOI: 10.1039/C7RA05874H

Yadav, S., & Singh, J.D., (2018). Synthesis and preliminary biological evaluation for the anticancer activity of organochalcogen (S/Se) tethered chrysin based organometallic Ru^{II}(η6–p–cymene) complexes, *J. Biomol. Struct. Dyn..*, (Accepted). https://doi.org/10.1080/07391102.2018.1513867.

Yuan, C.-Li., Zhang, A.-Guo., Zheng, Ze-Bo., & Wang, Ke-Z., (2013). The effects of structural variations of thiophene-containing Ru(II) complexes on the acid–base and DNA binding properties, *J. Biomol. Struct. Dyn..*, *31*, 316-330. DOI: https://doi.org/10.1080/07391102.2012.698238

Yousuf, I., Bashir, M., Arjmand, F. & Tabassum, S. (2018).Multispectroscopic insight, morphological analysis and molecular docking studies of Cu based chemotherapeutic drug entity with Human Serum Albumin (HSA) and Bovine Serum Albumin (BSA). *J. Biomol. Struct. Dyn..*, (Accepted). https://doi.org/10.1080/07391102.2018.1512899

Zhang, P., & Sadler, P.J. (2017). Advances in the design of organometallic anticancer complexes. *J. Organomet. Chem., 839,* 5-14. DOI: https://doi.org/10.1016/j.jorganchem.2017.03.038